

The promotional effect of surface Ru decoration on the catalytic performance of Co-based nanocatalysts for guaiacol hydrodeoxygenation

Qiangqiang Xu, Yisheng Shi, Lan Yang*, Guoli Fan, Feng Li*

State Key Laboratory of Chemical Resource Engineering, Beijing Advanced Innovation Center for Soft Matter Science and Engineering, Beijing University of Chemical Technology, Beijing, 100029, China

ARTICLE INFO

Keywords:

Surface Ru decoration
Highly dispersed Co nanoparticles
Surface defects
Hydrodeoxygenation
Guaiacol

ABSTRACT

In the present work, carbon-supported Ru-decorated Co-based nanocatalysts were fabricated via a layered double hydroxide/carbon composite precursor approach and applied to the efficient hydrodeoxygenation (HDO) of guaiacol to produce cyclohexanol. It was demonstrated that uniform and highly dispersed Co nanoparticles could be formed on the carbon matrix, and the decoration of a small amount of Ru on the surface of Co nanoparticles could introduce stronger hydrogenolysis active sites. Furthermore, the reduction temperature for catalyst precursors could tune the size of Co-containing nanoparticles and regulate the density of surface oxygen vacancies originating from CoO_x species. Under the mild reaction conditions (200 °C and 1.0 MPa hydrogen pressure), as-fabricated Ru-Co/C catalyst obtained at the reduction temperature of 600 °C showed excellent catalytic activity in the HDO of guaiacol, with a high cyclohexanol yield of ~94 %, which was attributable to surface exposure of highly dispersive Ru^0 sites and the formation of abundant defective oxygen vacancies. The present results provide a new approach for designing high-performance Co-based HDO nanocatalysts by both the surface decoration of small amounts of precious metals and the introduction of surface defective structures.

1. Introduction

In the recent decades, because accelerated consumption of fossil leads to major global concerns with respect to the finite reserves and environmental pollution, new and effective “energy strategy” for sustainable development of society and economy has become an urgent need in the world [1]. In this regard, there is an immediate need for sustainable energy sources and corresponding conversion technologies to substitute the conventional nonrenewable petroleum-based fuels [2]. For instance, as a renewable carbon source, the efficient catalytic conversion of a wide range of biomass sources into diverse high value-added chemical feedstocks and fuels has sprouted widely varied research attention [3,4]. In addition to the cellulosic fraction of biomass, the lignin fraction is also a useful but more challenging resource to produce high-value aromatic compounds [5]. Due to abundant carbon-oxygen bonds in lignin-based compounds, selective C—O cleavage through hydrodeoxygenation (HDO) processes becomes more critical [6]. As one of the main phenolic monomers obtained from lignin depolymerization, guaiacol with both types of carbon-oxygen bonds is a typical model molecule for the HDO research [7,8].

In earlier studies, noble metals (e.g. Ru, Pd, Pt and Re) are commonly

used in the HDO processes of lignin-derived phenols [9–11]. Besides, other relatively cheap transition metals, such as Mo, Ni, Fe, Co, Cu, and W [12–16], are also widely explored, despite their relatively low HDO activities. Among them, a large amount of research has focused on cobalt-based catalysts, since the flexible change in chemical valence states of Co species can affect the adsorption/activation of oxygen atoms in phenolic compounds, thus causing unique catalytic HDO activities of these Co-based catalysts [17–21]. For instance, Liu and coworkers reported that the particle size and the dispersion of Co were strongly dependent on the support [22]. Besides, the introduction of a second transition metal would improve their performance [23–26]. It was reported that compared with monometallic Co-based catalyst, $\gamma\text{-Al}_2\text{O}_3$ supported bimetallic NiCo one with a Ni/Co molar ratio of 1:3 could afford higher guaiacol conversion up to 96.1 % at 200 °C, along with the production of cyclohexanol as the main product, despite severe reaction conditions including 5.0 MPa hydrogen pressure and long reaction time [27]. Additionally, the addition of few Re into Co-based catalysts was beneficial to the HDO of phenol, which was attributed to the improved reducibility of Co species and the generation of additional active hydrogenation sites [28]. Therefore, for cobalt-based catalysts, the high dispersion of Co species and the introduction of small amounts of

* Corresponding authors.

E-mail addresses: yanglan@mail.buct.edu.cn (L. Yang), lifeng@mail.buct.edu.cn (F. Li).

<https://doi.org/10.1016/j.mcat.2020.111224>

Received 2 July 2020; Received in revised form 11 September 2020; Accepted 13 September 2020

Available online 25 September 2020

2468-8231/© 2020 Elsevier B.V. All rights reserved.

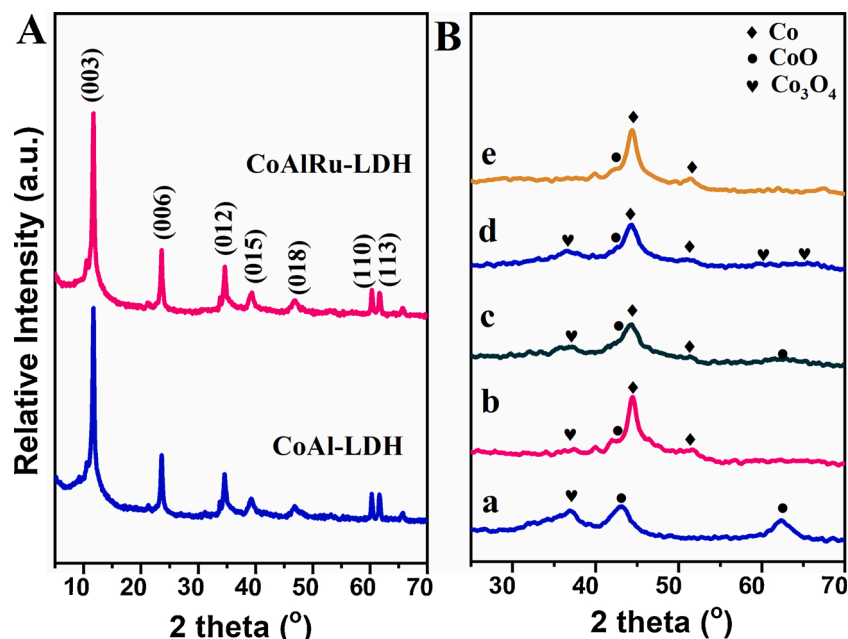


Fig. 1. XRD patterns of (A) LDH/C composite precursors and (B) different supported Co-based catalysts obtained at different reduction temperatures: (a) Co/C-500, (b) Co/C-600, (c) Ru-Co/C-500, (d) Ru-Co/C-600, (e) Ru-Co/C-700.

precious metals should be two crucial factors promoting their catalytic HDO activity for lignin-based phenolics.

On the other side, two-dimensional layered double hydroxides (LDHs) are a family of layered compounds with different metal cations (M^{2+} and M^{3+}) uniformly distributing within the brucite $Mg(OH)_2$ -like layers [29]. Interestingly, through the heating treatment and the following reduction process, LDHs can be topologically transformed into a broad range of supported metal-based catalysts with highly dispersive active metal sites and high specific surface areas [30]. Interestingly, LDH-derived supported Ni-based catalysts with the highly dispersed Ni nanoparticles (NPs) of 3 ~ 10 nm in size were reported to catalyze the breaking of $C_{aromatic}-O$ bond in anisole at 280 °C [31]. And, some Cu-containing LDHs were utilized to precisely prepare Cu-based catalysts applied in the HDO of biomass-derived compounds to gain higher catalytic performances [32,33].

Inspired by highly active Ru-based catalysts in the upgrading of lignin-derived phenolic compounds, in this study, we mainly focus on developing new high-performance carbon-supported Ru-decorated Co-based nanocatalysts through combining a small amount of Ru with a cheaper first-row transition metal Co to induce surface exposure of highly dispersive Ru^0 sites. The results demonstrated that the surface decoration of a small amount of Ru on Co NPs could significantly improve the catalytic performance of Co-based catalysts, and the as-fabricated Ru-Co/C catalyst obtained at a reduction temperature of 600 °C showed excellent catalytic performance for the guaiacol HDO process to generate cyclohexanol under the mild reaction conditions (200 °C and 1.0 MPa hydrogen pressure), with a high cyclohexanol yield of ~94 %. Further, the high catalytic efficiency of Ru-Co/C catalysts was found to be closely associated with the surface synergy between highly dispersive active Ru^0/Co^0 sites and abundant defective oxygen vacancies.

2. Experimental section

2.1. Catalyst preparation

2.1.1. Synthesis of samples

CoAlRu-LDH precursors were prepared by a coprecipitation route [34]. Typically, $Co(NO_3)_2 \cdot 6H_2O$ (12.5 mmol) and $Al(NO_3)_3 \cdot 9H_2O$

(6.25 mmol) were ultrasonically dispersed in deionized water (120 ml) containing an appropriate amount of $RuCl_3$ to get a clear solution. Then, an 80 ml of basic solution containing NaOH (40.0 mmol) and Na_2CO_3 (6.23 mmol) was used to titrate the above salt solution with stirring until pH was around 9.0. After aging at 90 °C for 18 h under nitrogen atmosphere, the CoAlRu-LDH precipitate was washed and dried overnight at 70 °C. In addition, CoAl-LDH was obtained without the addition of $RuCl_3$.

CoAlRu-LDH/C composites were assembled by a glucose-induced hydrothermal method [35]. Briefly, CoAlRu-LDH (3.59 g) and glucose (4.22 g) was added into a Teflon-lined stainless-steel reactor with 50 ml deionized water. Then, the resulting suspension was aged at 150 °C for 10 h. The CoAlRu-LDH/C composite precipitate was filtered, washed, and dried under vacuum at room temperature. For comparison, CoAl-LDH/C and ZnAlRu-LDH/C composite precursors were assembled under the same procedure as for CoAlRu-LDH/C composite.

CoAl-LDH/C, CoAlRu-LDH, and ZnAlRu-LDH/C composites were reduced under pure H_2 flow (100 ml min^{-1}) at 500, 600, or 700 °C, respectively, and held for 3 h. Then, the resulting samples were subjected to the passivation under N_2 flow with 1% O_2 for 1 h at room temperature. The obtained supported metal samples are denoted as Ru-Co/C-T, Co/C-T, and Ru/C-600, where T represents the applied reduction temperature. At last, the obtained samples were switched into in a sealed sample quartz tube filled with nitrogen gas for further characterization and catalytic tests.

2.2. Sample characterization

X-ray diffraction (XRD) patterns of samples were recorded on Shimadzu XRD-6000 diffractometer using the $Cu K\alpha$ source. The content of metals was analyzed on Shimadzu ICPS-7500 inductively coupled plasma atomic emission spectroscopy (ICP-AES). N_2 adsorption-desorption isotherms were obtained from Micromeritics ASAP 2460 sorptometer apparatus. The specific surface area was calculated by the BET method, and the date of pore structure were obtained according to the BJH method through desorption isotherms. Transmission electron microscopy (TEM) and high-angle annular dark-field scanning TEM-energy-dispersive X-ray spectroscopy (HAADF-STEM-EDX) were used to obtain the microstructural property of samples on JEOL JEM-2100

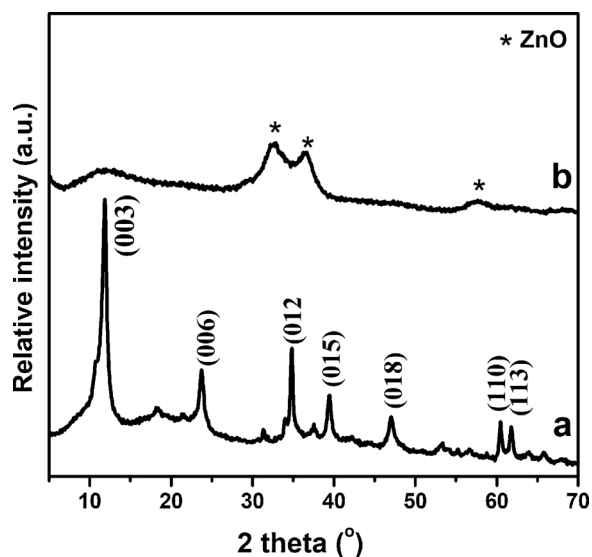


Fig. 2. XRD patterns of ZnAlRu-LDH/C composite precursor (a) and Ru/C-600 (b).

transmission electron microscope and HITACI S-5500 instrument. X-ray photoelectron spectroscopy (XPS) was collected through Thermo VG ESCALAB250 XPS spectrometer at the Al $K\alpha$ radiation. Before XPS measurement, the sample was transferred to a glove box filled with inert gas to make a testing sample, and then the tested sample was packaged

Table 1
Composition and textural properties of different samples.

Samples	Co ^a (wt %)	Al ^a (wt %)	Ru ^a (wt %)	S _{BET} ^b (m ² g ⁻¹)	D _p ^c (nm)	V _p ^d (cm ³ g ⁻¹)
Co/C-500	26.5	6.4	0	218	7.82	0.10
Co/C-600	31.5	6.4	0	259	6.16	0.14
Ru-Co/C-500	32.7	7.5	0.59	228	7.85	0.15
Ru-Co/C-600	35.5	6.7	0.48	232	10.14	0.20
Ru-Co/C-700	37.3	7.2	0.53	263	7.10	0.28

^a Determined by ICP-AES analysis.

^b BET specific surface area.

^c Average pore diameter.

^d Total volume of pores.

in the sealed sampler of the X-ray photoelectron spectrometer, in order to prevent further oxidation of samples at exposed air. Raman spectra were recorded through Mono Vista 2560 spectrometer using an excitation wavelength of 532 nm. Micromeritics ChemiSorb 2920 instrument was utilized to test H₂ temperature programmed desorption (H₂-TPD) of samples. *In situ* Fourier transform infrared (FT-IR) spectra for anisole adsorption were collected from Thermo Nicolet 380 FT-IR spectrometer. Before measurement, the sample was pretreated in Ar at 200 °C for 1 h. The powder sample was exposed to an atmosphere richer in anisole at room temperature for 30 min. Surface physically adsorbed anisole was removed by the Ar flow for 10 min.

2.3. Catalytic HDO test

The catalytic HDO reaction of guaiacol was conducted in a stainless-

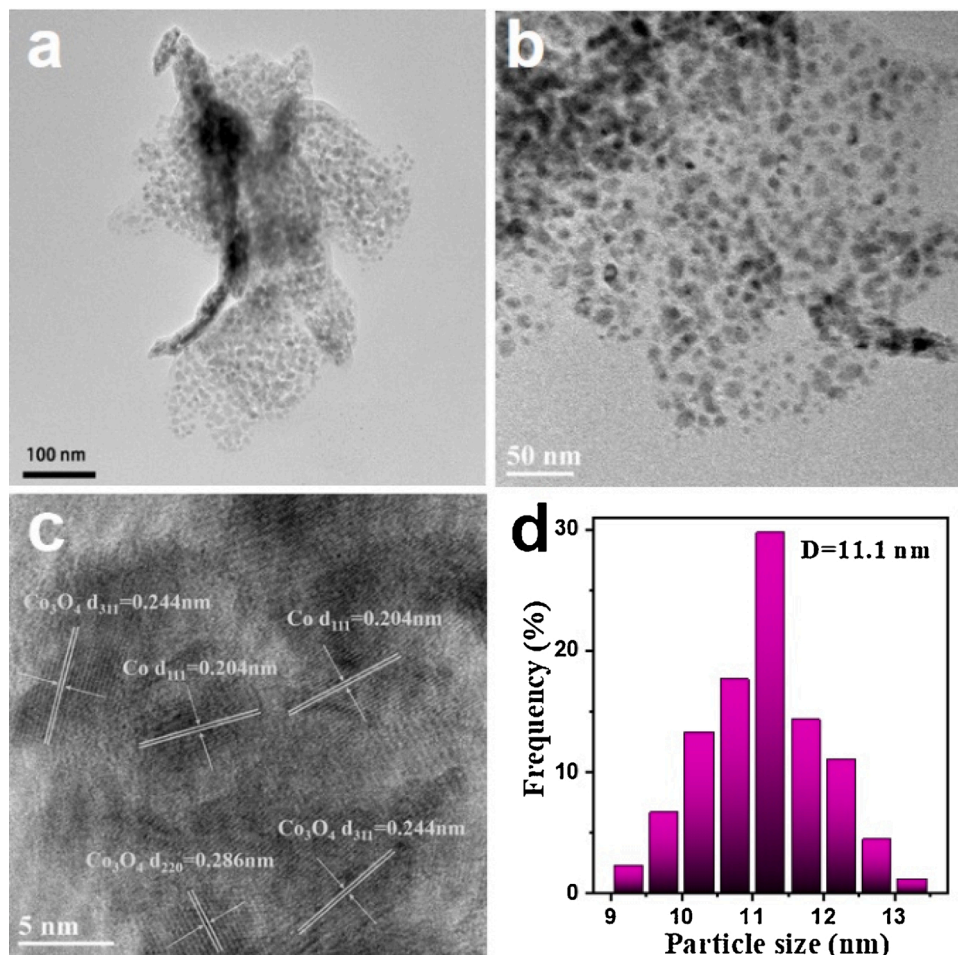


Fig. 3. TEM images (a and b), HRTEM image (c), and the particle size distribution histogram (d) of Ru-Co/C-600 sample.

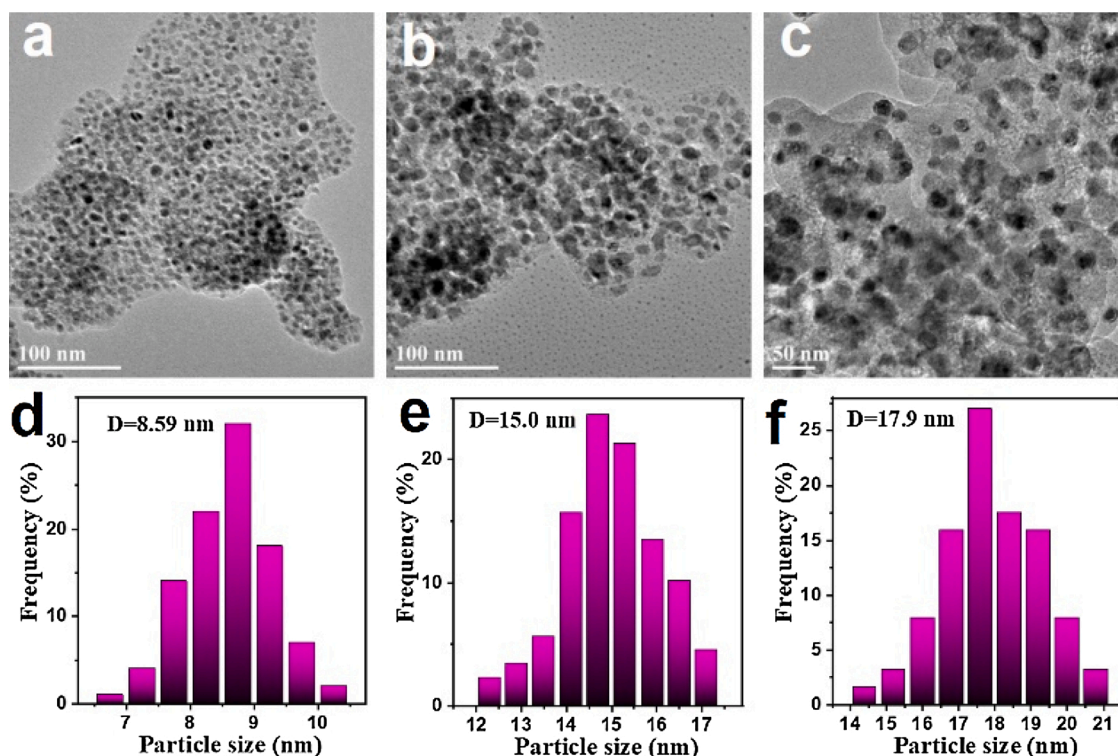


Fig. 4. TEM images and particle size distribution histograms of Ru-Co/C-500 (a,d), Ru-Co/C-700 (b,e), and Co/C-600 (c,f).

steel reactor (100 ml), where guaiacol (0.4 ml), *n*-decane (12 ml) and the catalyst (15 mg) were added. Firstly, the reactor was purged with nitrogen for five times. Then, the reactant was heated to a certain temperature and hydrogen gas was charged through continuous supply from the gas cylinder. Afterward, the reaction was initiated through vigorous magnetic stirring (800 rpm) at a certain H_2 pressure. After a desired time, the reactor was rapidly cooled down. At last, the products were analyzed by a gas chromatograph (Agilent GC7890B) equipped with DB-WAX capillary column (30.0 m \times 250 μ m \times 0.25 μ m) using flame ionization detector. In each case, the carbon balance was more than 95 %.

3. Results and discussion

3.1. Structure analysis of samples

As we know, XRD characterization can confirm the crystalline structure of samples. It is noted from Fig. 1A that XRD patterns of CoAl-LDH/C and CoAlRu-LDH/C samples show seven well-defined characteristic diffractions for a representative highly crystalline $Co_2Al(OH)_6(CO_3)_{0.5} \cdot H_2O$ phase (JCPDS 56-0954) [36]. No diffractions related to Ru-containing species and carbon materials can be observed, suggesting that Ru species may be successfully incorporated into the lattice of LDH precursor and carbon species can be combined with LDH phase in an amorphous form. After reduction of CoAlRu-LDH/C and CoAl-LDH/C samples, Ru-Co/C samples present a broad diffraction peak of (111) plane for metallic Co phase (JCPDS 89-7039) at about 44.4° (Fig. 1B), while the broad (311) diffraction for Co_3O_4 spinel phase (JCPDS 42-1467) and the weak (200) diffraction for CoO phase (JCPDS 43-1004) can be observed at 36.9° and 42.4° [37,38], respectively. The above diffraction peaks corresponding to metallic Co and Co oxides are broad, indicative of the character of small-sized Co-containing particles. And, no diffraction peaks assigned to crystalline Al_2O_3 are detected, demonstrating that Al species should exist in amorphous alumina form. Interestingly, different from Ru-Co/C-500, CoO and Co_3O_4 are the only two crystalline phases in the Co/C-500, strongly implying that the

introduction of a small amount of Ru species in CoAl-LDH can promote the reduction of Co species, probably due to the strong interactions between Ru and Co atoms. In all cases, no metallic Ru and other Ru-containing species are detected [39]. Furthermore, XRD patterns of Ru/C-600 reference sample derived from ZnAlRu-LDH/C precursor also reveal only the formation of ZnO phase (Fig. 2). The above results suggest that for Ru-containing reduced samples, no formation of Ru diffractions in XRD patterns is probably contributed to the much small Ru loading amount (~ 0.5 wt %) (Table 1).

Fig. 3 shows the typical TEM image of the representative Ru-Co/C-600. It is clearly seen that many small NPs are evenly distributed on a thin carbon sheet, and these NPs with an average size of about 11.1 nm present a narrow distribution of particle sizes. And, there are three types of the lattice fringes of interplanar spacings of 0.204, 0.244 and 0.286 nm, respectively, which match well with those of Co (111), Co_3O_4 (311), and Co_3O_4 (220) planes [40,41], confirming that Co species coexists in zero valence state and oxidation states. Meanwhile, TEM images of other Ru-Co/C samples depict similar results, despite the increasing size of NPs with the elevated reduction temperature (Fig. 4). In all cases, however, no lattice fringes related to the metallic Ru^0 phase can be observed [42], suggesting that Ru species may be homogeneously deposited onto the surface of Co particles because of the miscibility of two metals in bulk. In this regard, the formation of Co NPs with the larger average particle size (17.9 nm) in the case of Co/C-600 suggests that the surface decoration of Ru species may probably restrain the growth of metallic Co particles, thus inducing the formation of small-sized Co NPs. Further, HAADF-STEM images of representative Ru-Co/C-600 with elemental mapping and EDX line scanning spectra reveal a clear overlapping of surface Co and Ru species and a separation between Al and Co/Ru elements (Fig. 5), minor the similar surface distributions of Co and Ru elements, as well as their same positions on the surface. The above results confirm that Ru species can be homogeneously distributed over the surface of Co NPs, considering that the much lower content of Ru than that of Co.

XPS of $Co\ 2p_{3/2}$ and $O\ 1s$ regions was gained to determine surface electronic structures of Co and O elements on different samples (Fig. 6).

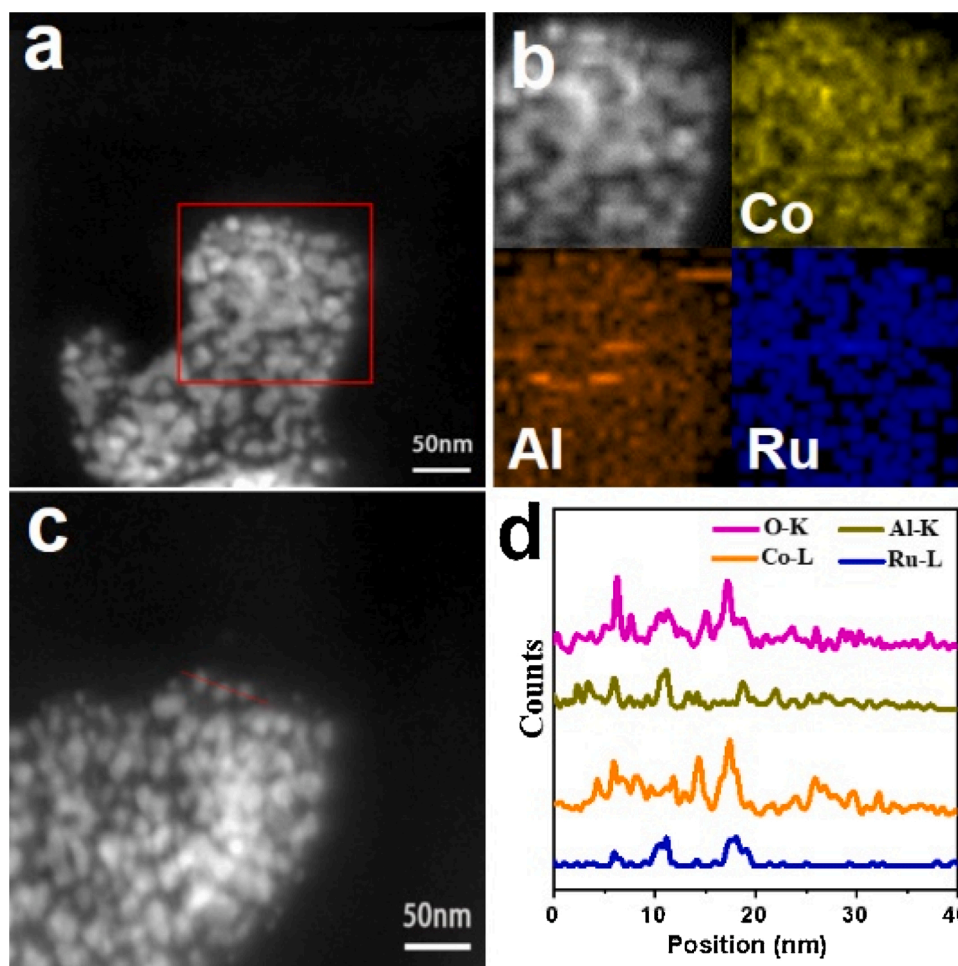


Fig. 5. HAADF-STEM images (a and c) of Ru-Co/C-600, the elemental EDX mapping (b) of O-K, Al-K, Co-K and Ru-K, and EDX line spectra of elements (d) along the red line in (c). (For interpretation of the references to colour in this figure legend, the reader is referred to the web version of this article).

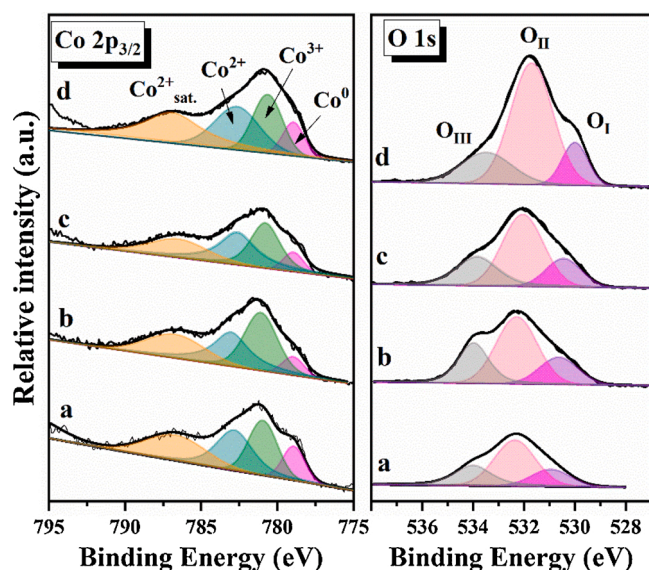


Fig. 6. XPS of Co $2p_{3/2}$ and O 1s regions for Co/C-600 (a), Ru-Co/C-500 (b), Ru-Co/C-600 (c), Ru-Co/C-700 (d) samples.

There are four deconvoluted peaks (778.7, 780.3, 782.7 and 786.5 eV) in the fine Co $2p_{3/2}$ spectra, which are associated with surface Co^0 , Co^{3+} , Co^{2+} species and shake-up Co^{2+} satellite [43], respectively. With the

Table 2

The surface element valence distribution of different supported Co-based catalysts obtained at different reduction temperatures.

Samples	Co (0) ^a (at %)	Co (III) ^a (at %)	Co(II) ^a (at %)	Co(II)/Co (III) ^b ratio	O _{II} / (O _I +O _{II}) ^b ratio	H ₂ uptake ^c (mmol/g)
Co/C-600	18.1	38.2	43.7	1.14	0.75	0.0386
Ru-Co/C-500	9.5	48.3	42.2	0.87	0.72	0.1560
Ru-Co/C-600	10.4	42.6	47.0	1.10	0.75	0.0822
Ru-Co/C-700	16.7	37.4	45.9	1.23	0.82	0.0427

^a Surface fractions of different Co species determined by XPS.

^b Determined by XPS of Co $2p_{3/2}$ or O1s region.

^c Determined by H₂-TPD profiles in the range of 50–400 °C.

elevated reduction temperature from 500 to 700 °C, surface $\text{Co}^{2+}/\text{Co}^{3+}$ intensity ratio increases gradually from 0.87 to 1.23 in the cases of Ru-containing samples (Table 2), while surface $\text{Co}^{2+}/\text{Co}^{3+}$ intensity ratio for Co/C-600 is almost equal to that for Ru-Co/C-600. Meanwhile, there are three deconvoluted contributions in the fine O 1s region, which are assigned to three types of O species: O_I (530.0–530.9 eV), O_{II} (531.7–532.3 eV), and O_{III} (533.5–533.9 eV), which are mainly associated with the lattice oxygen species in Co-containing oxides, the adsorbed oxygen species on defective sites (*i.e.* oxygen vacancies, Vo) or

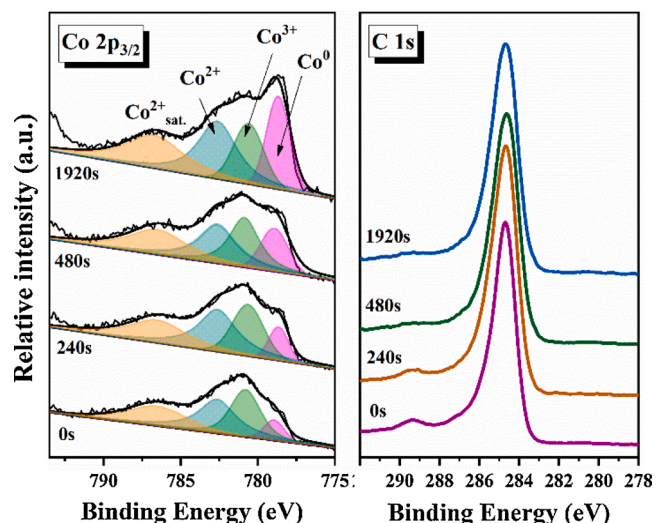


Fig. 7. Sputtering-XPS spectra of (a) Co $2p_{3/2}$ and (b) C 1s with Ru-Co/C-600.

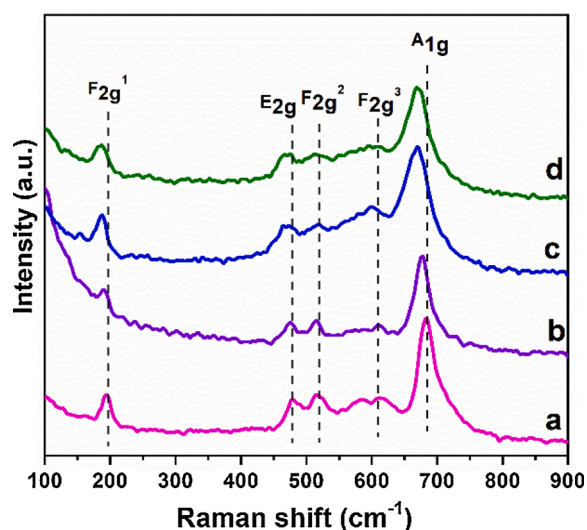


Fig. 8. Raman spectra of Ru-Co/C-500 (a), Co/C-600 (b), Ru-Co/C-600 (c), and Ru-Co/C-700 (d).

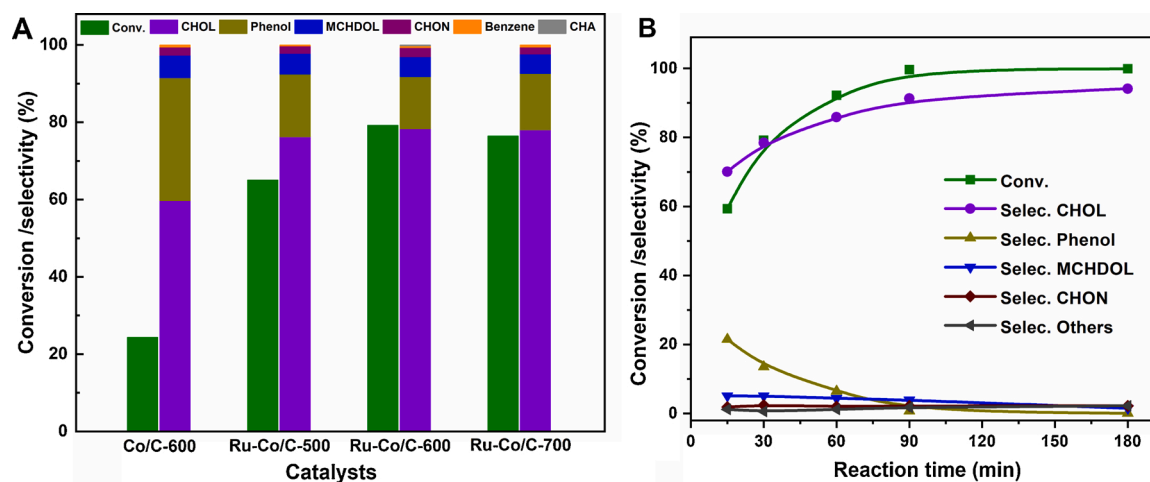


Fig. 10. (A) Catalytic performance for the HDO of guaiacol over different Co-based catalysts (200 °C, 1.0 MPa hydrogen pressure, and 0.5 h) and the change in the conversion and product selectivities with the reaction time over the Ru-Co/C-600 (B) (200 °C and 1.0 MPa hydrogen pressure).

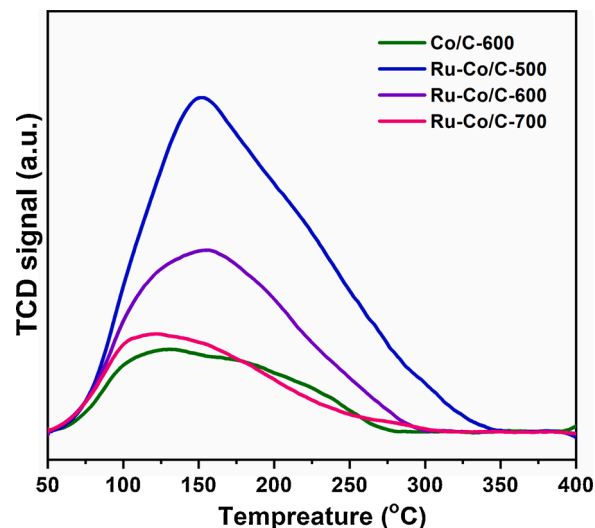


Fig. 9. H_2 -TPD profiles of different Co-based catalysts after reducing at different temperature.

hydroxyl species, and the surface oxygen species bonded to carbon atoms [40,44], respectively. As gathered in Table 2, the surface $O_{II}/(O_I+O_{II})$ intensity ratio slightly increases from Ru-Co/C-500 to Ru-Co/C-600 (Co/C-600) and Ru-Co/C-700. The above results imply that the formation of surface oxygen vacancies on as-fabricated Co-based samples in the form of $Co^{2+}-V_o-Co^{2+}$ defective structure, and that the higher reduction temperature is beneficial to the generation of more defective structures.

Based on the XPS results, in all cases, the surface fraction of metallic Co^0 in total Co species is below 20 %, which is completely different from the XRD result that metallic Co^0 is the main bulk crystalline phase in reduced samples. Therefore, one can suspect that surface CoO_x -decorated metal NPs may form on the surface of reduced samples. To prove this picture of such surface structure, Ru-Co/C-600 was tested by sputtering XPS analysis. As shown in Fig. 7, with the prolonging of sputtering time, the peak intensity of Co^0 $2p_{3/2}$ core level gradually exceeds that of cobalt oxide and becomes dominant. However, the $3d_{5/2}$ signal of Ru species cannot be detected at about 280 eV during XPS sputtering (Fig.7), due to the low Ru content. Meanwhile, the absence of $Ru3d_{5/2}$ signal also can rule out the possibility that Ru species are wrapped inside the core of Co particles or CoO_x species. The above results imply the formation of the core-shell structured Ru-Co@ CoO_x configuration on the

Table 3
Catalytic performance for hydrodeoxygenation over different reactants^a.

Reactants	Conv. (%)	Selectivity (%)				
		Benzene	CHOL	CHON	CHA	MCHDOL
anisole	72.4	7.2	22.5	0.5	26.9	42.9
phenol	97.8	0.7	97.3	1.8	1.3	0
cyclohexanone	100	0.5	99.2	0	0.3	0

^a Reaction condition: 200 °C; 1.0 MPa hydrogen pressure; 1.5 h.

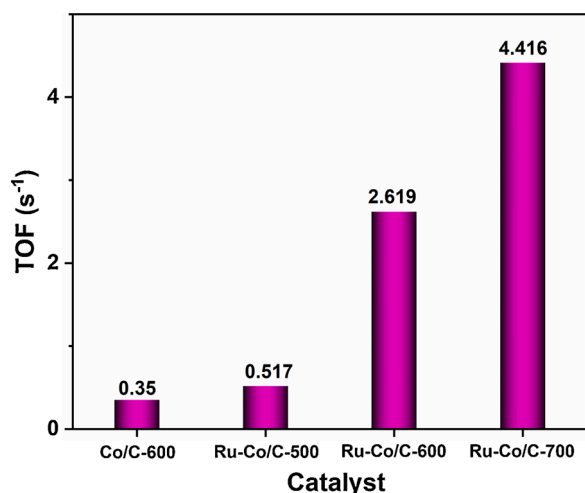


Fig. 11. The change of TOF value of guaiacol converted over different catalysts. Reaction conditions: 200 °C, 1.0 MPa hydrogen pressure, and 5 min.

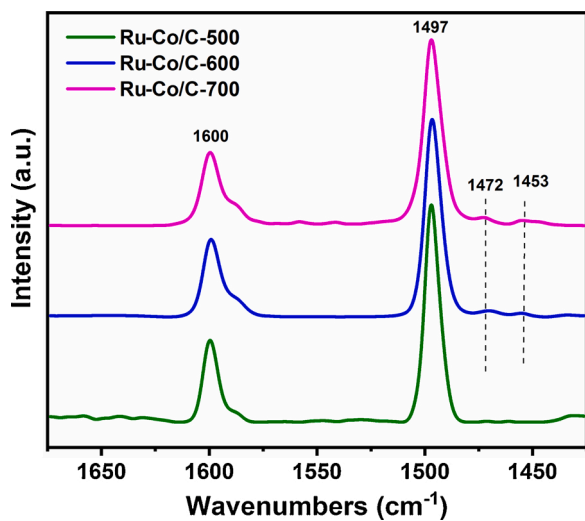


Fig. 12. In situ FT-IR spectra of anisole adsorbed on different Ru-Co/C catalysts at room temperature.

surface of Ru-Co/C-600 sample.

In order to further confirm the presence of surface defective structures, Raman spectra of supported Co-based samples were analyzed. As displayed in Fig. 8, five Raman peaks (186, 470, 511, 599, and 670 cm⁻¹) are assigned to F_{2g}¹, E_{2g}, F_{2g}², F_{2g}³, and A_{1g} vibrations of Co₃O₄ in spinel structure [45], respectively. Specifically, two F_{2g}¹ and A_{1g} vibrations are broadened and red-shift with the elevated reduction temperature, as well as the introduction of Ru, clearly demonstrating the enhanced defective structure of Co₃O₄ phase [46], due to the formation of more oxygen vacancies. Such surface oxygen vacancies are thought to be conducive to the adsorption and activation of oxygen-containing functional groups in phenolic compounds in the HDO reaction [47].

To get more insight into the dissociation hydrogen capacity of reduced samples, H₂-TPD was conducted. As shown in Fig. 9, the amount of H₂ uptake in the range of 50–400 °C decreases gradually in the following order: Ru-Co/C-500 > Ru-Co/C-600 > Ru-Co/C-700 > Co/C-600. Before TPD measurements, all Co-based samples were obtained by the reduction of H₂ above 500 °C. Therefore, the possible release of CO and CO₂ from carbon supports in the range of 50–500 °C during H₂-TPD process for reduced Co-based samples can be neglected. Here, the increased amount of H₂ uptake demonstrates the improved capacity of dissociation hydrogen, which originates from the enhanced dispersion of active Ru⁰/Co⁰ sites, consistent with the decrease in the size of Co or Ru-decorated Co NPs.

3.2. Catalytic HDO performance of Ru-decorated Co-based catalysts

The catalytic HDO reactions over different supported Co-based catalysts were conducted under 1.0 MPa hydrogen pressure at 200 °C. As presented in Fig. 10A, the catalytic activities of Ru-Co/C catalysts are remarkably better than that of Co/C-600 catalyst under the same reaction conditions. Especially, Ru-Co/C-600 catalyst delivers a guaiacol conversion of 79.2 % after a reaction of 0.5 h, with a cyclohexanol (CHOL) selectivity of 78.4 %. In striking contrast, Co/C-600 catalyst delivers much lower conversion of guaiacol (24.3 %) and cyclohexanol selectivity (59.8 %). Apparently, the introduction of a small amount of Ru (0.48 wt %) can greatly improve the catalytic HDO activity of Ru-Co/C-600, which mainly originates from the increased amount of active metallic sites responsible for the dissociation of molecular hydrogen. Meanwhile, compared with Ru-Co/C-600, Ru-Co/C-700 catalyst exhibits a slightly reduced activity, probably due to the presence of larger metal particles. On the other side, over the Ru-Co/C-600, the conversion and product selectivities changed with the reaction time (Fig. 10B). The guaiacol conversion rapidly increases within 90 min. Meanwhile, the cyclohexanol selectivity increases gradually, and the phenol selectivity decreases to zero. After a reaction of 3 h, the guaiacol conversion and the cyclohexanol selectivity reach about 99.6 % and 94.1 %, respectively. It demonstrates that the processes from guaiacol to phenol and from phenol to cyclohexanol are consecutive reactions. In general, even though previously reported Ru-containing catalysts with much higher loading amounts (above 5%) are effective for the HDO of guaiacol [48, 49], our Ru-Co/C catalyst systems with the much lower Ru loading of 0.48 % exhibit high activity, limiting the use of precious Ru by incorporating with a cheaper transition metal Co.

Further, anisole was used as the substrate to study the HDO reaction process over the present Ru-Co/C-600 catalyst (Table 3, entry 1). It is seen that no phenol is produced at 200 °C and 1.0 MPa after a reaction of 1.5 h, along with a small cyclohexanol selectivity of 22.5 %. However, as a result of hydrogenation-isomerization and dehydration reactions promoted by weak acidic sites on the catalyst surface [50], anisole also can be converted to a large amount of (cis- and trans-)-1-methyl-1,2-cyclohexanediol (MCHDOL) or cyclohexanone (CHON). Meanwhile, the product distributions using phenol as the substrate is consistent with those using guaiacol as the substrate (Table 3, entry 2). In two cases of anisole and guaiacol as substrates, phenolic hydroxyl can be hydrodeoxygenated to produce benzene. Furthermore, cyclohexanone used as the substrate can be easily converted into cyclohexanol under the same reaction conditions (Table 3, entry 3). The above results illustrate that the direct removal of the methoxy group from guaiacol is the first step of the HDO process.

In addition, the turnover frequency (TOF) for guaiacol conversion was calculated based on the moles of converted guaiacol per mole surface metallic sites determined by the H₂-TPD results after a reaction of 5 min, in order to identify the intrinsic catalytic activity of different catalysts. Notably, the TOF values over Ru-containing catalysts are larger than that over the Co/C-600 (0.35 s⁻¹) (Fig. 11). Especially, the TOF value over the Ru-Co/C-700 catalyst reaches as high as 4.416 s⁻¹, which is much higher than those over Ru-Co/C-500 (0.517 s⁻¹) and

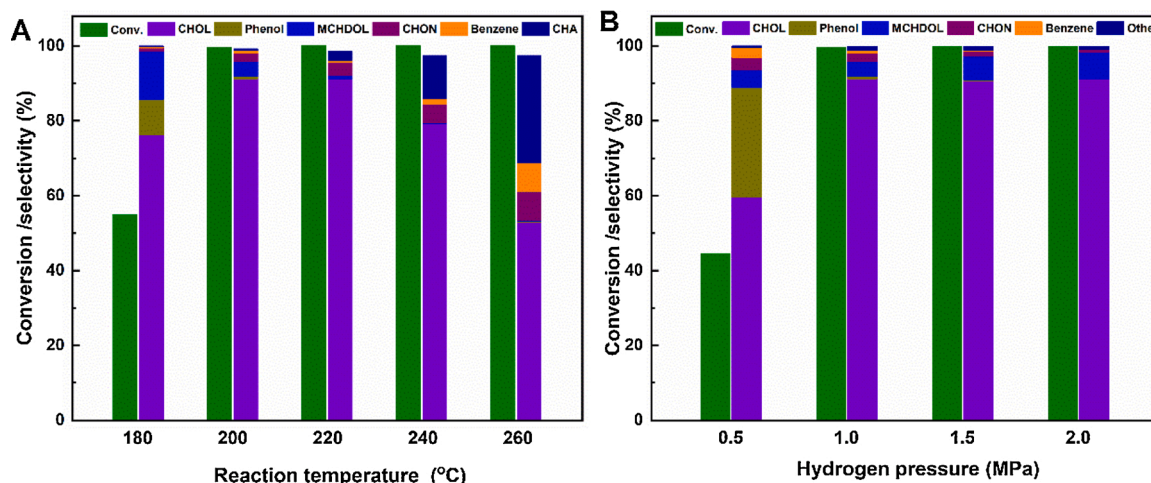


Fig. 13. Effect of reaction temperature (A) and hydrogen pressure (B) on the HDO of guaiacol over the Ru-Co/C-600 after 1.5 h. Reaction conditions: (a) 1.0 MPa hydrogen pressure; (b): 200 °C.

Table 4
Catalytic performance for hydrodeoxygenation over different reaction time^a.

Time	Conv. (%)	Selectivity (%)			
		Benzene	CHOL	CHON	CHA
5 min	99.8	1.4	73.8	3.7	18.8
180 min	99.8	0.2	20.5	0.2	77.0

^a Reaction condition: 260 °C; 2.0 MPa hydrogen pressure.

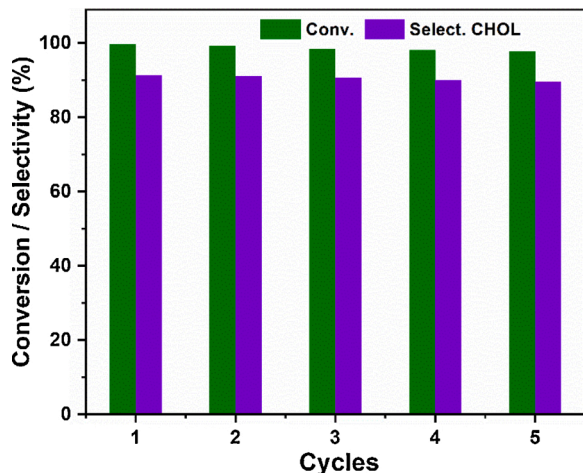
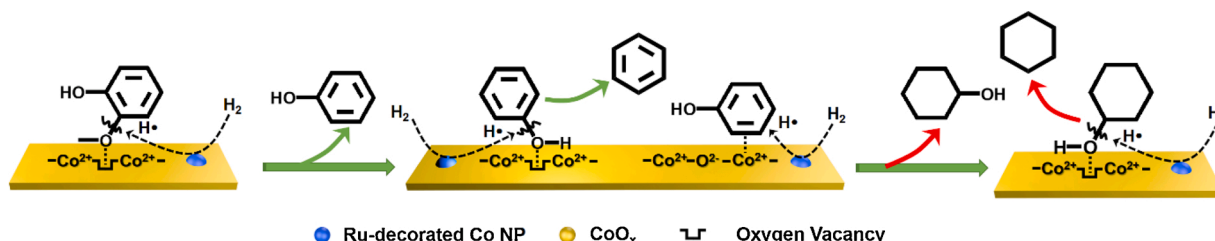


Fig. 14. Reusability of Ru-Co/C-600. Reaction condition: 200 °C, 1.0 MPa hydrogen pressure, and 1.5 h.



Scheme 1. Plausible reaction pathways and mechanism for the HDO of guaiacol over Ru-Co/C catalysts.

Ru-Co/600 (2.619 s^{-1}). Such significant TOF difference between these catalysts demonstrates that surface active metallic species are not the sole active reaction sites.

To get more information on the adsorption and activation of guaiacol on Ru-Co/C catalysts, in situ FT-IR spectra for adsorbed anisole on samples were collected (Fig. 12). The two absorption bands near 1600 and 1497 cm^{-1} are correlated with the C=C stretching vibration in the benzene ring. Meanwhile, in the cases of Ru-Co/C-600 and Ru-Co/C-700, the asymmetric and symmetric bending vibrations of the methoxy group of adsorbed anisole appear at 1472 and 1453 cm^{-1} , respectively. The above results imply that there is stronger chemical adsorption between the methoxy group of anisole and the surface of Ru-Co/C-600 and Ru-Co/C-700 through the interaction between surface Vo sites in CoO_x species and the lone electron pair of oxygen in methoxy group in anisole, by which the C_{ring}-O bond may be weakened. In our present Ru-Co/C catalyst system, highly dispersed surface Ru sites combined with metallic Co sites may more easily dissociate molecular hydrogen, and as-generated active hydrogen species can further rapidly transfer to the catalyst surface. In this case, surface Ru sites also may act as hydrogen transfer centers to significantly promote the HDO process through the hydrogen spillover from Co NPs to defective CoO_x. Meanwhile, a large amount of surface oxygen vacancies may act as adsorption/activation sites for guaiacol. Therefore, the surface synergy between highly dispersed Ru⁰/Co⁰ sites and oxygen vacancies greatly improves the intrinsic activity of Ru-Co/C catalysts, especially Ru-Co/C-700 with more surface oxygen vacancies.

The catalytic HDO performance of Ru-Co/C-600 catalyst as a function of the reaction temperature was assessed (Fig. 13a). With the extended reaction time up 1.5 h, the guaiacol conversion can reach as high as 99.6 % at 200 °C, with a high cyclohexanol selectivity of 91.3 %. With the decreasing reaction temperature from 200 °C to 180 °C, the guaiacol conversion decreases, while the selectivity to 1-methyl-1,2-cyclohexanediol and phenol increase to 12.8 % and 9.5 %, respectively.

respectively. On the contrary, upon increasing temperature from 180 to 260 °C, the amount of 1-methyl-1,2-cyclohexanediol or phenol is decreased sharply, while the selectivity of cyclohexanone, benzene, bicyclohexane and cyclohexane (CHA) gradually increases to 7.8, 7.7, 2.4 and 28.5 %, respectively. Nevertheless, the sharply increased cyclohexane selectivity is accompanied by the enhanced formation of cyclohexanone, benzene and bicyclohexane at the expense of cyclohexanol production, indicating that the as-fabricated Ru-Co/C catalysts can catalyze deoxygenation process of cyclohexanol at higher temperatures. To further explain the above results, the HDO reaction was also conducted at 260 °C and 2 MPa hydrogen pressure (Table 4). It is found that the main product is cyclohexanol with a yield of about 74.0 % after a reaction of 5 min, and the cyclohexane yield reaches 77 % after a reaction of 3 h. It demonstrates that higher reaction temperatures can favor the formation of cyclohexane. Different from the reaction temperature, the increase in the hydrogen pressure from 1.0–2.0 MPa cannot remarkably affect guaiacol conversion and product selectivities (Fig. 13b). At the pressure of 0.5 MPa, a large amount of phenol (29.4 %) can be produced. Clearly, the higher hydrogen pressure promotes both the ring-hydrogenation and the hydrogenolysis of the methoxy group in guaiacol to 1-methyl-1,2-cyclohexanediol, despite the constant selectivity of cyclohexanol. The reusability and stability of catalysts are quite important properties for heterogeneous catalysts. It is found that Ru-Co/C-600 still retains high catalytic activity even after five cycles (Fig. 14), indicating the excellent reusability of the catalyst.

Based on the above structural characterizations and catalytic experiments, reaction pathways and mechanism of the HDO of guaiacol over Ru-Co/C catalysts are proposed. As shown in Scheme 1, guaiacol is more susceptible to the C_{ring}-O cleavage, thus causing the formation of phenol and further the ring-hydrogenation. Meanwhile, phenol also can be converted into benzene through the removal of the phenolic hydroxyl group. Further, the removal of the alcoholic hydroxyl group in cyclohexanol can produce cyclohexane at higher reaction temperatures and hydrogen pressures. Especially, the removal of the methoxy group in guaiacol can be regulated by designing the structure of catalysts, as well as controlling the reaction conditions. Specifically, in the present Ru-Co/C catalyst system, active hydrogen species dissociated from surface highly dispersed metallic Ru⁰/Co⁰ sites may transfer to defective CoO_x, where oxygen-containing functional groups (e.g. methoxy group) in guaiacol can be to adsorbed and activated in the course of HDO process, thus greatly improving the catalytic HDO performance of catalysts.

4. Conclusions

In summary, carbon-supported Ru-decorated Co-based nanocatalysts were successfully prepared through a layered double hydroxide/carbon composite precursor approach. It was demonstrated that surface Ru-decorated Co NPs were surrounded by large amounts of defective CoO_x species. As-fabricated Ru-Co/C-600 catalyst obtained at the reduction temperature of 600 °C could afford a high cyclohexanol yield of ~94 % in the HDO of guaiacol at 200 °C and 1.0 MPa hydrogen pressure. It was found that cyclohexanol could further be transfer into cyclohexane at higher temperature of 260 °C and hydrogen pressure of 2.0 MPa. And, the surface decoration of a small amount of Ru greatly improved the reactivity of Ru-Co/C catalysts, since surface Ru sites could not only participate in the reaction as highly active sites for the dissociation of molecular hydrogen but also act as hydrogen transfer centers to significantly promote the HDO process through the hydrogen spillover from Co NPs to surface CoO_x defects. More importantly, abundant oxygen vacancies could promote the adsorption and activation of the methoxy group in guaiacol. Correspondingly, the surface synergy between highly dispersed Ru⁰/Co⁰ sites and oxygen vacancies could contribute to the greatly improved catalytic HDO performance of Ru-Co/C catalysts. Understanding the promotional effect of surface decoration of active Ru sites on less active non-precious metals can provide a new approach to design more efficient catalysts.

CRediT authorship contribution statement

Qiangqiang Xu: Investigation, Writing - original draft. **Yisheng Shi:** Investigation, Methodology. **Lan Yang:** Conceptualization, Writing - original draft. **Guoli Fan:** Visualization. **Feng Li:** Conceptualization, Formal analysis, Writing - review & editing.

Declaration of Competing Interest

The authors declare that they have no known competing financial interests or personal relationships that could have appeared to influence the work reported in this paper.

Acknowledgments

We thank gratefully the financial support from National Natural Science Foundation of China (21776017; 21991102; 21521005) and the Fundamental Research Funds for the Central Universities (XK1802-6).

References

- [1] X. Han, Y. Guo, X. Liu, Q. Xia, Y. Wang, *Catal. Today* 319 (2019) 2–13.
- [2] C. Ranga, R. Lødeng, V.I. Alexiadis, T. Rajkhowa, H. Björkan, S. Chytil, I. H. Svenum, J. Walmsley, C. Detavernier, H. Poelman, P. Van Der Voort, J. W. Thybaut, *Chem. Eng. J.* 335 (2018) 120–132.
- [3] T. Ennaert, J. Van Aelst, J. Dijkmans, R. De Clercq, W. Schutyser, M. Dusselier, D. Verboekend, B.F. Sels, *Chem. Soc. Rev.* 45 (2016) 584–611.
- [4] Y. Yang, W. Zhang, F. Yang, D.E. Brown, Y. Ren, S. Lee, D. Zeng, Q. Gao, X. Zhang, *Green Chem.* 18 (2016) 3949–3955.
- [5] D. Shi, L. Arroyo-Ramírez, J.M. Vohs, *J. Catal.* 340 (2016) 219–226.
- [6] Y.-B. Huang, L. Yan, M.-Y. Chen, Q.-X. Guo, Y. Fu, *Green Chem.* 17 (2015) 3010–3017.
- [7] C.-c. Chiu, A. Genest, A. Borgna, N. Rösch, *ACS Catal.* 4 (2014) 4178–4188.
- [8] A.L. Jongerius, R.W. Gosselink, J. Dijkstra, J.H. Bitter, P.C.A. Bruijninx, B. M. Weckhuysen, *ChemCatChem* 5 (2013) 2964–2972.
- [9] Y. Nakagawa, M. Ishikawa, M. Tamura, K. Tomishige, *Green Chem.* 16 (2014) 2197–2203.
- [10] H. Ren, C. Li, D. Yin, J. Liu, C. Liang, *RSC Adv.* 6 (2016) 85659–85665.
- [11] E.A. Roldugina, E.R. Naranov, A.L. Maximov, E.A. Karakhanov, *Appl. Catal. A Gen.* 553 (2018) 24–35.
- [12] Z. Cai, F. Wang, X. Zhang, R. Ahishakiye, Y. Xie, Y. Shen, *Mol. Catal.* 441 (2017) 28–34.
- [13] Q. Lu, C.-J. Chen, W. Luc, J.G. Chen, A. Bhan, F. Jiao, *ACS Catal.* 6 (2016) 3506–3514.
- [14] T.N. Phan, C.H. Ko, *Catal. Today* 303 (2018) 219–226.
- [15] A.A. Smirnov, S.A. Khromova, D.Y. Ermakov, O.A. Bulavchenko, A.A. Saraev, P. V. Aleksandrov, V.V. Kaichev, V.A. Yakovlev, *Appl. Catal. A Gen.* 514 (2016) 224–234.
- [16] J. Zhang, B. Fidalgo, A. Kolios, D. Shen, S. Gu, *Chem. Eng. J.* 336 (2018) 211–222.
- [17] X. Liu, L. Xu, G. Xu, W. Jia, Y. Ma, Y. Zhang, *ACS Catal.* 6 (2016) 7611–7620.
- [18] T. Mochizuki, S.-Y. Chen, M. Toba, Y. Yoshimura, *Appl. Catal. B: Environ.* 146 (2014) 237–243.
- [19] I.D. Mora-Vergara, L. Hernández Moscote, E.M. Gaigneaux, S.A. Giraldo, V. G. Baldovino-Medrano, *Catal. Today* 302 (2018) 125–135.
- [20] T.M. Sankaranarayanan, A. Berenguer, C. Ochoa-Hernández, I. Moreno, P. Jana, J. M. Coronado, D.P. Serrano, P. Pizarro, *Catal. Today* 243 (2015) 163–172.
- [21] N.T.T. Tran, Y. Uemura, S. Chowdhury, A. Ramli, *Appl. Catal. A Gen.* 512 (2016) 93–100.
- [22] X. Liu, W. Jia, G. Xu, Y. Zhang, Y. Fu, *Selective ACS Sustain. Chem. Eng.* 5 (2017) 8594–8601.
- [23] D.P. Gamliel, S. Karakalos, J.A. Valla, *Appl. Catal. A Gen.* 559 (2018) 20–29.
- [24] A.A. Smirnov, Z. Geng, S.A. Khromova, S.G. Zavarukhin, O.A. Bulavchenko, A. A. Saraev, V.V. Kaichev, D.Y. Ermakov, V.A. Yakovlev, *J. Catal.* 354 (2017) 61–77.
- [25] H. Taghvaei, M.R. Rahimpour, P. Bruggeman, *RSC Adv.* 7 (2017) 30990–30998.
- [26] J. Zhang, B. Fidalgo, S. Wagland, D. Shen, X. Zhang, S. Gu, *Fuel* 238 (2019) 257–266.
- [27] M. Zhou, J. Ye, P. Liu, J. Xu, J. Jiang, *ACS Sustain. Chem. Eng.* 5 (2017) 8824–8835.
- [28] I.T. Ghampon, C. Sepúlveda, A.B. Dongil, G. Pecchi, R. García, J.L.G. Fierro, N. Escalona, *Catal. Sci. Technol.* 6 (2016) 7289–7306.
- [29] J. Feng, Y. He, Y. Liu, Y. Du, D. Li, *Chem. Soc. Rev.* 44 (2015) 5291–5319.
- [30] G. Fan, F. Li, D.G. Evans, X. Duan, *Chem. Soc. Rev.* 43 (2014) 7040–7066.
- [31] X. Zhang, Xiao Chen, S. Jin, Z. Peng, C. Liang, *ChemistrySelect* 1 (2016) 577–584.
- [32] N. Pino, G. Hincapie, D. Lopez, *Ing. Invest* 37 (2017) 34–42.
- [33] Z. Gao, F. Liu, L. Wang, F. Luo, *Appl. Surf. Sci.* 480 (2019) 548–556.
- [34] M.Y. Miao, J.T. Feng, Q. Jin, Y.F. He, Y.N. Liu, Y.Y. Du, N. Zhang, D.Q. Li, *RSC Adv.* 5 (2015) 36066–36074.
- [35] R. Han, C. Nan, L. Yang, G. Fan, F. Li, *RSC Adv.* 5 (2015) 33199–33207.
- [36] Y. Zhao, F. Li, R. Zhang, D.G. Evans, X. Duan, *Chem. Mater.* 14 (2002) 4286–4291.

- [37] C. Cui, G. Du, K. Zhang, T. An, B. Li, X. Liu, Z. Liu, J. Alloys. Compd. 814 (2020), 152239.
- [38] M.K. Gnanamani, G. Jacobs, H.H. Hamdeh, W.D. Shafer, F. Liu, S.D. Hopps, G. A. Thomas, B.H. Davis, ACS Catal. 6 (2016) 913–927.
- [39] M. Lu, H. Du, B. Wei, J. Zhu, M. Li, Y. Shan, J. Shen, Ind. Eng. Chem. Res. 56 (2017) 12070–12079.
- [40] W. Li, G. Zhang, X. Jiang, Y. Liu, J. Zhu, F. Ding, Z. Liu, X. Guo, C. Song, ACS Catal. 9 (2019) 2739–2751.
- [41] M.K. Gnanamani, G. Jacobs, R.A. Keogh, W.D. Shafer, D.E. Sparks, S.D. Hopps, G. A. Thomas, B.H. Davis, Appl. Catal. A Gen. 499 (2015) 39–46.
- [42] Y. Li, J. Abbott, Y. Sun, J. Sun, Y. Du, X. Han, G. Wu, P. Xu, Appl. Catal. B: Environ. 258 (2019), 117952.
- [43] L.F. Liotta, G. Di Carlo, G. Pantaleo, A.M. Venezia, G. Deganello, Appl. Catal. B: Environ. 66 (2006) 217–227.
- [44] W. Cao, W. Luo, H. Ge, Y. Su, A. Wang, T. Zhang, Green Chem. 19 (2017) 2201–2211.
- [45] X. Wang, Y. Liu, T. Zhang, Y. Luo, Z. Lan, K. Zhang, J. Zuo, L. Jiang, R. Wang, ACS Catal. 7 (2017) 1626–1636.
- [46] Bd. Rivas, R. Lopez-Fonseca, C. Jimenez-Gonzalez, J.I. Gutierrez-Ortiz, J. Catal. 281 (2011) 88–97.
- [47] Z. Gao, L. Yang, G. Fan, F. Li, ChemCatChem 8 (2016) 3769–3779.
- [48] A.A. Dwiatmoko, I. Kim, L. Zhou, J.-W. Choi, D.J. Suh, J. Jae, J.-M. Ha, Appl. Catal. A Gen. 543 (2017) 10–16.
- [49] M. Ishikawa, M. Tamura, Y. Nakagawa, K. Tomishige, Appl. Catal. B: Environ. 182 (2016) 193–203.
- [50] J. Chang, T. Danuthai, S. Dewiyanti, C. Wang, A. Borgna, ChemCatChem 5 (2013) 3041–3049.